Published in final edited form as:
ACS Nano. 2019 January 22; 13(1): 163–175. doi:10.1021/acsnano.8b05067.

A Self-Healing, All-Organic, Conducting, Composite Peptide Hydrogel as Pressure Sensor and Electrogenic Cell Soft Substrate

Priyadarshi Chakraborty[†,iD], **Tom Guterman**[†], **Nofar Adadi**[‡], **Moran Yadid**[†], **Tamar Brosh**[§], **Lihi Adler-Abramovich**[§,iD], **Tal Dvir**[†,‡,iD], and **Ehud Gazit**[*,†,‡,iD]

[†]Department of Molecular Microbiology and Biotechnology, George S. Wise Faculty of Life Sciences, Tel Aviv University, Tel Aviv 6997801, Israel

[§]Department of Oral Biology, The Goldschleger School of Dental Medicine, Sackler Faculty of Medicine, Tel Aviv University, Tel Aviv 6997801, Israel

[‡]Department of Materials Science and Engineering, Iby and Aladar Fleischman Faculty of Engineering, Tel Aviv University, Tel Aviv 6997801, Israel

Abstract

Conducting polymer hydrogels (CPHs) emerge as excellent functional materials, as they harness the advantages of conducting polymers with the mechanical properties and continuous 3D nanostructures of hydrogels. This bicomponent organization results in soft, all-organic, conducting micro-/nanostructures with multifarious material applications. However, the application of CPHs as functional materials for biomedical applications is currently limited due to the necessity to combine the features of biocompatibility, self-healing, and fine-tuning of the mechanical properties. To overcome this issue, we choose to combine a protected dipeptide as the supramolecular gelator, owing to its intrinsic biocompatibility and excellent gelation ability, with the conductive polymer polyaniline (PAni), which was polymerized *in situ*. Thus, a two-component, all-organic, conducting hydrogel was formed. Spectroscopic evidence reveals the formation of the emeraldine salt form of PAni by intrinsic doping. The composite hydrogel is mechanically rigid with a very high storage modulus (G') value of ~2 MPa, and the rigidity was tuned by changing the peptide concentration. The hydrogel exhibits ohmic conductivity, pressure sensitivity, and, importantly, self-healing features. By virtue of its self-healing property, the polymeric nonmetallic hydrogel can reinstate its intrinsic conductivity when two of its macroscopically separated blocks are rejoined. High cell viability of cardiomyocytes grown on the composite hydrogel demonstrates its noncytotoxicity. These combined attributes of the hydrogel allowed its utilization for dynamic range pressure sensing and as a conductive interface for

[iD]**ORCID**
Priyadarshi Chakraborty: 0000-0001-7174-7660
Lihi Adler-Abramovich: 0000-0003-3433-0625
Tal Dvir: 0000-0002-3153-9928
Ehud Gazit: 0000-0001-5764-1720

[*]**Corresponding Author:** (E.G.) ehudg@post.tau.ac.il.

Notes
The authors declare no competing financial interest.

Europe PMC Funders Author Manuscripts

electrogenic cardiac cells. The composite hydrogel supports cardiomyocyte organization into a spontaneously contracting system. The composite hydrogel thus has considerable potential for various applications.

Keywords

peptide; conducting hydrogel; self-healing; conductivity; pressure sensing; cardiac cells

Hydrogels are three-dimensional (3D) solid-like materials in which supramolecular or polymeric micro- or nanostructures entangle to immobilize water. These structures can be biocompatible, with some bearing striking resemblance to natural tissues, such as the extracellular matrix.1,2 Hydrogels are therefore considered promising candidates for the development of biological applications and specifically for tissue engineering purposes.3,4 Compared to conventional cross-linked polymeric hydrogels, supramolecular hydrogels are stimuli-responsive, their properties can be more easily modulated, and they do not require any additional cross-linking.5 Moreover, supramolecular hydrogels are typically free from reagents, such as initiators, enzymes, or catalysts that may be present in cross-linked polymeric hydrogels and potentially bear cytotoxic or other undesired effects on tissue regeneration.6 Short peptides have been demonstrated to be efficient low molecular weight supramolecular hydrogelators as they confer excellent propensity of unidirectional amide H-bonding.7–11 Indeed, over the past decade, short peptide based supramolecular hydrogels have emerged as promising materials for biotechnology and biomedical applications.12–15

Conducting polymers (CPs) show multiple properties which make them excellent candidates for biomedical applications, including their organic nature, responsiveness to external stimuli, possible functionalization by biomolecules, electrical conductivity, *etc.*16 Indeed, CPs have been employed as conducting substrates to support the proliferation of cardiac cells, which are naturally responsive to electrical stimuli.17 However, the extremely low intrinsic mechanical stiffness of CPs hinders their practical applications. A simple approach to engineer mechanically stiff CP-based materials is their integration with hydrogels, to obtain conducting polymer hydrogels (CPHs).18–22 CPHs combine the advantages of CPs with the mechanical stiffness of hydrogels, resulting in intrinsically conducting 3D objects with underlying micro-/nanostructures,23 which can bridge biological and synthetic systems. Owing to their electrical conductivity, CPHs are useful for bioelectronic applications, including biosensors, for medical and biodevices, and for controlling electrical stimuli-responsive cells.24–28 It was previously reported that incorporation of conductive inorganic nanomaterials (such as gold nanoparticles and gold nanowires) into otherwise insulating, conventional cardiac tissue engineering scaffolds resulted in faster and more synchronized electrical signal propagation in the engineered tissues due to the enhanced electrical coupling between the neighboring cardiac cells.29 Thus, CPHs could be promising scaffolds for this application, providing an all-organic, continuous conducting path compared to the noncontinuous, point-to-point connected conducting networks of inorganic nanoparticles. Moreover, self-healing CPHs are excellent candidates for cardiac cell delivery vehicles. The self-healing property aids in enduring the mechanical load arising from the

Europe PMC Funders Author Manuscripts

contraction of the heart, thereby improving the vehicle's lifetime.28 Hence, the design of CPHs exhibiting self-healing ability could be helpful for various biomedical applications.

Although this is an active field of research, the application of CPHs as functional biomaterials is still limited. This is due to the lack of coexistence of beneficial attributes in a single CPH, including adequate mechanical properties for culturing soft tissues, self-healing behavior, and sufficient biocompatibility. To tackle this issue, we chose a peptide-based supramolecular gelator to impart a gel state because of the general intrinsic noncytotoxicity and excellent tunable gelation ability of such gelators. Moreover, we hypothesized that the carboxylic acid groups of the peptide could potentially serve as a dopant of the conducting polymer chains. On the basis of this rationale, we designed a composite hydrogel based on the well-studied *N*-fluorenylmethoxycarbonyl diphenylalanine (Fmoc-FF) hydrogelator and the conductive polymer polyaniline (PAni), a product of *in situ* aniline (Ani) polymerization. PAni was chosen due to its facile synthesis, environmental stability, excellent conductivity, and biocompatibility.30,31 The Fmoc-FF-PAni composite hydrogels were mechanically strong and electrically conducting and could self-heal. Moreover, these hydrogels exhibited pressure-responsive conductance, as demonstrated by the fabrication of a pressure sensor device. Finally, the composite hydrogels proved to be noncytotoxic and were able to support the growth of electrical stimuli-responsive cardiac cells. This work presents the Fmoc-FF-PAni hydrogel as a functional composite material that possesses a range of beneficial properties for various applications.

Results and Discussion

Formation and Characterization of the Fmoc-FF-PAni Hydrogels

Composite Fmoc-FF-PAni hydrogels were formed by employing the solvent-switch method. Fmoc-FF was solubilized in dimethyl sulfoxide (DMSO) and diluted with an aqueous solution of aniline (Ani), forming the nearly transparent Fmoc-FF-Ani hydrogel at an Fmoc-FF:Ani molar ratio of 1:5 (Figure 1a). This molar ratio was maintained in all experiments, unless otherwise mentioned. Next, Fmoc-FF-Ani hydrogel was subjected to oxidative polymerization by ammonium persulfate (APS) solution yielding the Fmoc-FF-PAni hydrogel, which presented a deep green color, characteristic of PAni (Figure 1a). Transmission electron microscopy (TEM) studies revealed that the Fmoc-FF-Ani hydrogels comprise interconnected fibers (Figure 1b,c), similar to pure Fmoc-FF hydrogels (Figure S1). However, after polymerization of aniline, the morphology was notably different (Figure 1d,e). While the overall network structure was retained, the Fmoc-FF-PAni hydrogels displayed a significantly increased fiber diameter, of ~10 nm, as demonstrated by quantitative analysis (Figure S2a,b). This increase can be attributed to the formation of PAni nanostructures, which possibly act as a shell around the core assembly of Fmoc-FF (Scheme 1).32,33 One noteworthy aspect of the Fmoc-FF-PAni fibers is their coarse surface, quite contrary to the Fmoc-FF-Ani fibers. On the Fmoc-FF-PAni fibers resided granular particulates, which had likely formed due to heterogeneous nucleation of PAni.34 This type of granules on the fiber surface were also observed previously in a polypyrrole-based hydrogel.35

To ascertain the formation of PAni and to investigate the secondary structure of the Fmoc-FF component, dried hydrogels of Fmoc-FF and Fmoc-FF-PAni (Fmoc-FF concentration = 0.5% (w/v)) were analyzed using Fourier transform infrared (FTIR) spectroscopy (Figure 1f). The amide I peaks of Fmoc-FF at 1694 and 1655 cm^{-1} were assigned to the stacked carbamate group of the Fmoc moiety and to the imperfect stacking of the amide groups, respectively.36 Interestingly, the peak positions remained similar in the case of Fmoc-FF-PAni, implying that polymerization does not affect the core assembly of the peptide. In addition, several signature peaks of PAni appeared in the Fmoc-FF-PAni hydrogels as a consequence of polymerization (Table S1).37 Analysis of the FTIR stretching vibrations demonstrated the phenomena of doping, i.e., polaron generation. PAni, in its emeraldine base form, exhibits a peak at 1160 cm^{-1}, corresponding to the vibration mode of the quinoid structure (N═Q═N; Q = quinoid). In the Fmoc-FF-PAni hydrogels, this peak was blue-shifted to 1147 cm^{-1}, signifying the loss of the double bond character due to polaron generation (Q═N^+H—B or B—N^+H—B; B = benzenoid).38 The ratio of the relative intensities of quinoid to benzenoid ring modes (I_q/I_b) was calculated to be 1.14, also indicating that, in the Fmoc-FF-PAni hydrogels, the percentage of imine units is higher than that of amine units and that the PAni is in a highly conducting form.39

Taken together, the observations thus far suggest a probable mechanism for the formation of Fmoc-FF-PAni fibers. When the Fmoc-FF-Ani fibers come into contact with APS, the $S_2O_8^{2-}$ ions react with the Ani monomers that are presumably associated with the surface of the Fmoc-FF fibers, oxidizing them to cation radicals. These cation radicals then act as seeds onto which PAni chains grow gradually.18 This creates a sheath of PAni chains over the core assembly of Fmoc-FF fibers (Scheme 1) that leads to their thickening.32,33 Finally, the PAni shells allow for heterogeneous nucleation of PAni to occur, leading to coarsening of the fibers.34

Next, we analyzed and compared the concentration-dependent UV–vis spectra of Fmoc-FF and Fmoc-FF-Ani (Figure S3). Fmoc-FF exhibited three characteristic peaks at 264, 292, and 304 nm, and no significant shift of these peaks were observed with an increase in the concentration (Figure S3a). However, in the case of Fmoc-FF-Ani (Figure S3b), a small red shift in the 264 nm peak was observed. A comparison of UV–vis spectra of Fmoc-FF and Fmoc-FF-Ani (Fmoc-FF concentration = 0.1% (w/v) for both) presented in Figure S3c revealed that the Fmoc-FF-Ani exhibited a small red shift of the Fmoc-FF-originating 264 nm peak. The small red shift could be attributed to enhanced π-stacking interactions. It also suggests a possible coassembly formation between Fmoc-FF and Ani. As for the final Fmoc-FF-PAni hydrogel, the UV–vis spectra of its pulverized suspension in ddH_2O showed the characteristic peaks of PAni (Figure 1g). The bands at 273, 422, and 783 nm were ascribed to the π–π^* transition in the benzenoid rings, polaron band-π^* band, and π-band-polaron band transition of doped PAni chains, respectively.37 These peaks indicate polaron formation by doping, as well as the formation of PAni in its highly conducting, emeraldine salt form.

Concentration-dependent fluorescence spectra Fmoc-FF and Fmoc-FF-Ani hydrogels are depicted in Figure S4a,b. Fmoc-FF, at a concentration of 0.05% (w/v), exhibited an emission peak at 320 nm which could be ascribed to the presence of antiparallel Fmoc-FF dimers

(Figure S4a).40 With an increase in concentration (i.e., during gelation), the intensity of this peak increased with a small red shift (2 nm) signifying effective π-stacking interactions. In the case of the Fmoc-FF-Ani hydrogels (Figure S4b), similar behavior is observed, although the red shift is much more pronounced (17 nm). Similar to UV–vis spectra, a small red shift in emission maxima could be observed at lower concentrations as well (between Fmoc-FF concentration of 0.05% and 0.1% (w/v)). A comparison of the fluorescence spectra of Fmoc-FF and Fmoc-FF-Ani hydrogels at 0.5% (w/v) concentration (Figure S4c) revealed that the fluorescence peak for the antiparallel dimer structures decreased in intensity for the Fmoc-FF-Ani hydrogel and also red-shifted. The red shift of the peak may signify enhanced π-stacking during coassembly formation in the Fmoc-FF-Ani hydrogels, whereas the decreased fluorescence intensity may result from the incorporation of nonfluorescent Ani in the Fmoc-FF hydrogels.41 Interestingly the fluorescence of the hydrogels is almost entirely quenched after the polymerization of aniline, as observed from the fluorescence spectra of Fmoc-FF-PAni hydrogels (Figure S4c, inset).

Mechanical Properties of the Hydrogels

Adequate mechanical rigidity of conducting hydrogels is an important requirement for practical applications. To examine their mechanical properties, rheological studies were performed on Fmoc-FF-PAni hydrogels at a Fmoc-FF concentration of 2% (w/v), while retaining the 1:5 molar ratio of Fmoc-FF:Ani. Furthermore, to ascertain the effect of Ani polymerization on the mechanical properties of the hydrogels, we performed rheological analysis on the Fmoc-FF and Fmoc-FF-Ani hydrogels at a Fmoc-FF concentration of 2% (w/v). At first, strain sweep experiments (1 Hz frequency) were carried out on the hydrogels to determine the linear viscoelastic regime (Figure S5a–c). It was observed that Fmoc-FF, Fmoc-FF-Ani, and Fmoc-FF-PAni hydrogels exhibited breakage at 13%, 70%, and 11% strain, respectively. The increased breakage strain in the Fmoc-FF-Ani hydrogels may result from the formation of coassembly domains between Fmoc-FF and Ani in the hydrogel state. Given their increased diameter and polymerized shells, the Fmoc-FF-PAni fibers are likely more rigid, and accordingly they could not withstand higher strain values and displayed decreased breakage strain.42

Figure 2a–c depicts the dynamic frequency sweep experiment carried out on the Fmoc-FF, Fmoc-FF-Ani, and Fmoc-FF-PAni hydrogels at 0.1% strain, demonstrating a wide linear viscoelastic regime. For all hydrogels, the storage modulus (G') was almost one order of magnitude higher than the loss modulus (G'') over the frequency region tested, and the G' value was independent of the frequency, confirming the viscoelastic nature of the hydrogels (plot of tan δ vs angular frequency of the Fmoc-FF-PAni hydrogel is provided in Figure S5d). Interestingly, the G' values of the corresponding hydrogels, measured at an angular frequency of 10 rad/s, increased in the order Fmoc-FF (0.3 MPa) < Fmoc-FF-Ani (0.7 MPa) < Fmoc-FF-PAni (2 MPa). The improved G' value for the Fmoc-FF-Ani hydrogels resulted from the coassembled domains of Fmoc-FF and Ani in the hydrogel state. Further improvement of G' for the Fmoc-FF-PAni hydrogels resulted from the formation of rigid PAni chains, capable of storing energy more efficiently.32

Interestingly, the G' value of the Fmoc-FF-PAni hydrogel (~2 MPa) is considerably higher than that of other self-assembled supramolecular gels43,44 and strong peptide-based hydrogels45–49 and comparable to several biological tissues.50

Temperature sweep experiments carried out on the Fmoc-FF-PAni hydrogels (Figure 2d) demonstrated the invariability of G' and G'' over a temperature range of 20–100 °C. As no crossover of the modulus values was observed, it can be inferred that the hydrogels did not exhibit breakage at the mentioned temperature range and that they were stable under biologically relevant temperatures. Additionally, Figure 2e depicts the shear viscosity vs shear rate plot of the Fmoc-FF-PAni hydrogels, exemplifying its shear-thinning property, which can be attributed to the shear-induced breaking of the Fmoc-FF-PAni networks.

Next, we opted for the tuning of mechanical properties of the Fmoc-FF-PAni hydrogels by altering the concentration of the Fmoc-FF gelator. Frequency sweep experiments were carried out on Fmoc-FF-PAni hydrogels with Fmoc-FF concentrations of 0.5%, 1%, 1.5%, and 2% (w/v), and the G' values were plotted with angular frequency (Figure 2f). The G' values (at 10 rad/s angular frequency) were calculated to be 0.01, 0.09, 0.3, and 2 MPa for the Fmoc-FF-PAni hydrogels with a Fmoc-FF concentration of 0.5%, 1%, 1.5%, and 2% (w/v), respectively. Therefore it is obvious that the mechanical properties of the Fmoc-FF-PAni hydrogels could be successfully tuned by altering the concentration of the Fmoc-FF gelator.

Self-Healing Property of the Composite Hydrogels

To establish the hydrogel's self-healing nature, a step strain experiment was conducted. The Fmoc-FF-PAni hydrogel was subjected to five cycles of time sweep experiments with low (0.1%) and high (100%) strain values (Figure 2g). At 100% strain, the hydrogels were converted to a quasi-liquid (sol) state, as evident from the modulus values ($G' < G''$). When the strain was reduced to 0.1% (i.e., in the linear viscoelastic regime), the gel reformed again ($G' > G''$). This behavior was consistent over multiple cycles, indicating the reproducibility of the self-healing nature. We have also performed the continuous step strain measurements on the Fmoc-FF and Fmoc-FF-Ani hydrogels under identical conditions (Figure S5e,f) to examine their self-healing ability. It was evident that both Fmoc-FF and Fmoc-FF-Ani hydrogels exhibited self-healing properties. Therefore, it can be surmised that the self-healing property of the Fmoc-FF-PAni hydrogels is attributable to Fmoc-FF. Furthermore, aiming to visually demonstrate its self-healing capability, a monolith of the Fmoc-FF-PAni hydrogel was cut into two blocks which were then fused together. The blocks joined within 5 min without the aid of any external healing agent (Figure 2h). We similarly observed that when two separate blocks of Fmoc-FF (semitransparent) and Fmoc-FF-PAni (dark) hydrogels were fused, the blocks joined without any external healing agent (Figure 2i). This behavior of heterogeneous fusion clearly demonstrates the excellent self-healing ability of the Fmoc-FF hydrogel, which is shared by the Fmoc-FF-PAni hydrogel. As rheological results proved that the self-healing ability of the Fmoc-FF-PAni hydrogels had stemmed from Fmoc-FF, it can be concluded that Fmoc-FF fibers possess the inherent tendency to re-entangle after they are detached by mechanical force or separation, and this property remains intact after Ani polymerization. This re-entanglement results from the strong supramolecular

interactions acting among the fibers.51 When two blocks of the Fmoc-FF-Pani hydrogels or two heterogeneous blocks of Fmoc-FF and Fmoc-FF-PAni hydrogels were fused, the dynamic nature of the self-healing process allowed the re-entanglement of the fibers at the fusion interface, thus triggering the healing.

Conducting Properties of the Composite Hydrogels

As evident from the spectroscopic analyses, the PAni produced in the hydrogels is adequately doped. As a consequence, Fmoc-FF-PAni hydrogels are expected to present high conductivity. Indeed, the current–voltage (*I*–*V*) curves of Fmoc-FF-PAni hydrogels dried between gold electrodes resembled nearly ohmic behavior in the measured voltage range (Figure 3a). A DC conductance of 0.5 mS was obtained for the Fmoc-FF-PAni hydrogels from the slope of the *I*–*V* curves. In contrast, a control of Fmoc-FF-Ani hydrogels exhibited no change in current when the voltage was varied, behaving like a typical insulator (Figure 3a). In the Fmoc-FF-PAni dried hydrogels, sufficient doping of the PAni chains created radical cations/holes (polarons), which can freely move along the PAni chains, making them intrinsically metallic-like in nature. Here, the PAni chains grew unidirectionally along the surface of the self-assembled peptide backbone, bestowing a metallic-like nature to the Fmoc-FF-PAni nanofibers. The bulk conductivity of the hydrated Fmoc-FF-PAni hydrogels was demonstrated by serially connecting a light-emitting diode (LED) to the hydrogel discs, which allowed the activation of the LED by closing the circuit (Figure 3b,c).

Self-Healing Conductivity

As the Fmoc-FF-PAni hydrogels exhibited a self-healing property, we were interested to examine whether they could reinstate their conductivity after macroscopic separation and rejoining of gel monolith blocks. For this purpose, a LED was serially connected to an Fmoc-FF-PAni monolith, which enabled the activation of the former (Figure 3d). The monolith was then macroscopically separated into two blocks, resulting in disconnection of the circuit and deactivation of the LED (Figure 3d). The two blocks were then fused together, and following their rejoining, the LED was reactivated (Figure 3d). To further establish the restoration of conductivity after the cutting and rejoining procedure, we measured the resistance change of the Fmoc-FF-PAni hydrogel monoliths during the healing process (Figure 3e). It was observed that the resistance values increased upon the cutting of the hydrogel monolith into two pieces and reached the instrumental limit (20 MΩ). However, when the two pieces were fused, the resistance decreased and reached similar values as obtained before the cutting procedure. Therefore, it is evident that the Fmoc-FF-PAni hydrogel reinstated its conductivity after self-healing. Thus, the Fmoc-FF-PAni hydrogels not only retain their mechanical integrity but also reinstate their bulk conductivity after macroscopic disruption.

Electrochemical Analysis of the Composite Hydrogel

Cyclic voltammetry (CV) was performed to investigate the electrochemical stability of the Fmoc-FF-PAni hydrogels. The cyclic voltammograms of Fmoc-FF-PAni hydrogel (Figure 4a) exhibited two sets of electrochemical oxidation and reduction peaks (C_1/A_1 and C_2/A_2). The first redox peak (C_1/A_1) correspond to transition from leucoemeraldine to conducting emeraldine state of PAni fiber networks, whereas the Faradaic transition from the emeraldine

to the pernigraniline state of PAni networks was designated by the second redox peak (C_2/A_2).27,52 In addition, Figure 4b shows high capacity retention of ~89% after 1000 cycles. Overall, the data indicates stable and nearly repeatable redox properties of the Fmoc-FF-PAni hydrogel system during cyclic performance.

Composite Hydrogel for the Construction of Pressure Sensors

The ability of amyloid fibril aerogels functionalized with gold nanoparticles to function as pressure sensor devices has been recently demonstrated.53 Here, the combined elasticity and conductivity of the Fmoc-FF-PAni hydrogels was utilized for the construction of a pressure sensor device, free of metals in its active sensing component. The device was based on the change of bulk resistance of the Fmoc-FF-PAni hydrogels as a function of applied pressure (Figure 4c; see Figure S6 for plotted conductivity). The resistance of the hydrogel decreased with increasing pressure and nearly regained its original value when the pressure was completely released. This change in resistance values was repeatable for the 16 steps tested (Figure 4d). This further attests to the robustness of the Fmoc-FF-PAni hydrogel and shows its applicability for pressure sensing.

The sensitivity of the device was calculated using the equation $S = \mathrm{d}R/\mathrm{d}P$, where R and P denote the resistance and applied pressure, respectively.54 When sensitivity (S) was plotted against pressure (Figure S7), it manifested a power law dependence similar to that of resistance vs pressure. More detailed analysis (Figure S7, inset) revealed that, at pressure values < 330 Pa, the device exhibited an S value of ~15–51 kPa^{-1}. However, at pressure values > 5.5 kPa, the sensitivity decreased to 1 kPa^{-1}. In comparison, an S value of 0.43–0.24 k Pa^{-1} was exhibited by a hydrogel comprised of alginate and flexible SiO_2 nanofibers. 55 A polypyrrole based hydrogel exhibited an S value of ~7.7–41.9 kPa^{-1} and 0.4 kPa^{-1} at pressures < 100 Pa and > 1 kPa, respectively.54 Therefore, the S values obtained from the Fmoc-FF-PAni hydrogel are comparable with those of previously reported sensors.

Stability of the Fmoc-FF-PAni Hydrogels under Physiologically Relevant Conditions

Next, we investigated the stability of the Fmoc-FF-PAni hydrogels under physiologically relevant conditions. We first tested its conductance following incubation in cell culture media for 2 weeks. A conductance value of 0.8 mS was obtained, which is comparable to that of the nontreated hydrogel, suggesting that the cell culture medium does not significantly alter the conductance of the Fmoc-FF-PAni hydrogels. We next subjected Fmoc-FF-PAni hydrogels to enzymatic degradation. Hydrogel discs (8 mm diameter) were incubated with culture medium containing collagenase type II (1 U/mL) enzyme for 20 days at 37 °C, and their residual weights were measured after a two-day interval. A slow rate of degradation was observed, and a total degradation of ~62% was obtained after 20 days (Figure S8), indicating the stability of the hydrogel under these conditions.

Composite Hydrogels as a Soft Substrate for Growth of Cardiac Cells

Another potential application of the Fmoc-FF-PAni hydrogel may be for assisting in recording the electrical activity of cells. Scaffolds with nanofibrous architecture strongly resemble the extracellular matrix of the myocardium and can accordingly confer the support necessary for cardiac cells.56–58 Additionally, cardiomyocytes are electrogenic cells with

the ability to spontaneously contract under electrical signal propagation.59,60 While growing cardiac cells, the cells must transfer electrical signals rapidly and effectively. Culturing cells in nonconducting hydrogel scaffolds could prevent propagation of the electrical signal, leading to nonsynchronous contraction. Hence, appropriate design of biomaterials capable of mimicking the extracellular matrix of the myocardium necessitates both nanofibrous architecture and conductivity.

It was previously reported that 3D porous polymeric scaffolds obtained from alginate61 or poly(lactic acid)62 can organize cardiac cells into functioning tissues, although their low conductivity restricts the contraction of the patches as a unit due to the absence of electrical coupling between the neighboring cells.63 Cardiac cells become rounded and lose their gap junction proteins after their seeding within the scaffolds, which, in turn, disturbs anisotropic transfer of the electric signals. To avoid this issue, it was necessary to improve the electric communication between the cardiac cells by introducing conducting nanomaterials in the otherwise insulating scaffolds. For this purpose, inorganic and carbon nanomaterials were incorporated in the conventional tissue engineering scaffolds, resulting in faster and synchronized electrical signal propagation of the engineered tissues.29,64–66 Graphene oxide nanoparticle-incorporated conducting hybrid hydrogels also led to enhanced activity and maturity of the cardiomyocytes in comparison to its pure nonconducting counterpart.67 Therefore, the conducting, nanofibrous, and elastic Fmoc-FF-PAni hydrogel should support the growth and function of cardiomyocytes.

We hypothesized that the conductivity of the hydrogel, together with its elasticity, may be utilized for interfacing electrogenic cells with electrodes. Currently, to measure the electrical activity of cells, such as neurons or cardiomyocytes, the cells are seeded and cultured on pristine metal electrodes, such as gold or platinum. Although these materials accurately measure the activity of the cells, their mechanical properties do not match the mechanical properties of native tissues,68 which may limit the function of the cells. Therefore, we sought to evaluate the potential of the Fmoc-FF-PAni hydrogel to serve as a soft substrate for cells. For this purpose, we chose the Fmoc-FF-PAni hydrogels with an Fmoc-FF concentration of 0.5% (w/v), as their mechanical properties may be suitable for culturing soft tissues. First, to rule out any cytotoxic effect, we performed cell viability assay on cardiomyocytes seeded on the surface of Fmoc-FF-PAni hydrogels (Fmoc FF concentration = 0.5% (w/v)) after 7 days (Figure 5a). Such a cultivation period is enough for cell attachment and elongation.69 Cell viability was quantified using an ImageJ plugin to quantify the number of nuclei stained with propidium iodide (PI) and with Hoechst. The PI-positive nuclei count indicates the number of dead cells, and Hoechst-positive nuclei count indicates the total number of cells. Viability was quantified as the ratio between the PI-negative nuclei to Hoechst-positive nuclei. Viability on Fmoc-FF-PAni hydrogels (Fmoc-FF concentration = 0.5% (w/v)) was 69 ± 1.3%, as quantified from two independent samples and four field of views (FOVs) per sample. For the control conditions, Fmoc-FF hydrogels disintegrated in the cell culture conditions and Fmoc-FF-Ani hydrogels did not support cell viability, as demonstrated by % viability close to zero (data not shown). In comparison, alginate scaffolds exhibited 80% cell viability for nearly 2 weeks.61 It was also shown that incorporation of gold nanowires within alginate scaffolds did not show cytotoxic effects on cardiac cells.29 In order to improve the cell viability of Fmoc-FF-PAni system, further

optimization is still in progress. Next, the ability of the conducting hydrogel to support cardiomyocyte maturation on its surface was assessed. Cardiac cells were isolated from the ventricles of neonatal rats and seeded on the surface of the Fmoc-FF-PAni hydrogels (Fmoc-FF concentration = 0.5% (w/v)) at different molar ratios of Fmoc-FF and Ani (Fmoc-FF: Ani = 1:1, 1:3, 1:5). However, since the cells did not attach to the hydrogels containing lower PAni concentrations, we used the Fmoc-FF-PAni hydrogels with 1:5 Fmoc-FF:Ani molar ratio. As shown by immunostaining, seven days post-seeding the cells were spread on the hydrogel surface and exhibited an elongated morphology with pronounced actinin striation and troponin-t expression (Figure 5b). Cell spreading and elongation suggest that this hydrogel is compatible with cardiomyocyte culture. To assess elongation and spreading of cardiomyocytes, we quantified nuclear morphology. It was previously shown that nuclear shape is correlated to cell shape and controlled by the cytoskeletal actin filaments. Versaevel *et al.* and Bray *et al.* have demonstrated spatial coordination between cell and nuclear shape in endothelial cells and in cardiomyocytes.70,71 Using micropatterning techniques they have demonstrated that when cells were not allowed to elongate and hence maintained circular or square shape, the nuclei were also more circular and randomly aligned. However, when cells were spread on elongated patterns the nuclei exhibited more elongated morphology and were oriented with the direction of the cells. In these studies, nuclear morphology was quantified and correlated to cellular morphology. We quantified the following nuclear morphological parameters (Figure 5c–f): (1) Nuclear radius ratio, defined as the ratio between a, the long/major axis of an ellipse, to b, the short/minor axis of an ellipse. This value equals 1 for a circle and >1 for an ellipse. (2) Eccentricity, defined as $e = \sqrt{1 - \frac{b^2}{a^2}}$. For a perfect circle this value equals zero, and for an ellipse the value will be <1, whereas the more elongated the shape is, the closer to 1 the eccentricity. (3) Nuclear shape index (NSI) is defined as $\mathrm{NSI} = \frac{4\pi A}{P^2}$, where A is the nuclear area and P is the perimeter. For a perfect circle NSI = 1, and for an ellipse NSI < 1, with smaller values corresponding to more elongated shapes. For cardiomyocyte nuclei that were seeded on Fmoc-FF-PAni hydrogels (Fmoc-FF concentration = 0.5% (w/v)), the mean radius ratio was 1.94 ± 0.38, mean eccentricity was 0.84 ± 0.06, and mean NSI was 0.91 ± 0.06. These values are in accordance with values reported by Versaevel *et al.* and Bray *et al.* for cells patterned on 1:4–1:7 aspect ratio rectangles (i.e., elongated cells).70,71

To further assess the function of the cultured cells on the Fmoc-FF-PAni (Fmoc-FF concentration = 0.5% (w/v)) substrate, the cells were incubated with a calcium-sensitive dye. Calcium transient imaging of the cells revealed their spontaneous and synchronous contraction (Movie S1). Analysis of the recording at five separate sites along the hydrogel revealed a propagation of the calcium wave through the sample, indicating the ability of the hydrogel to support functional cell growth and the formation of an electrically connected cardiac tissue (Figure 5g,h).

Next, we tried to test the viability, spreading, and contractile functions of cardiomyocytes on Fmoc-FF-PAni hydrogels of different stiffnesses. However, the Fmoc-FF-PAni hydrogels with higher Fmoc-FF concentrations tested (1% and 2% (w/v)) did not support cell viability,

as demonstrated by % viability close to zero on these samples (data not shown). Hence, it is evident that a particular stiffness, as well as concentration of the scaffold material, is necessary for adequate cardiomyocyte function.

We can now provide a probable mechanism of the attachment of cardiomyocytes on the Fmoc-FF-PAni hydrogels (Fmoc-FF concentration = 0.5% (w/v)) with high PAni content. PAni-based composite fibers have previously been utilized for cardiac tissue engineering. Electrospun PAni containing gelatin fibers were used for the attachment, migration, and proliferation of H9c2 rat cardiac myoblasts.72 Nanofibrous sheets composed of poly(L-lactic acid) and PAni showed promoting effect on the differentiation of H9c2 cardiomyoblasts.52 Therefore, it is clear that PAni could facilitate the attachment of cardiomyocytes on the nanofiber surface. The probable reason behind the attachment of cardiomyocytes with PAni is related to the hydrophilicity of PAni nanofiber surfaces73 and interactions between positively charged PAni chains74,75 and the negatively charged cells. In this case, the sheathing of PAni chains on the Fmoc-FF assemblies confers hydrophilicity and positive charge to the composite fibers. Therefore, the Fmoc-FF-PAni hydrogels with the highest PAni content (molar ratio of Fmoc-FF:Ani = 1:5) possessed the adequate surface properties for the attachment of cardiomyocytes. Once the cardiomyocytes are attached to the surface of the composite fibers, they can mature and exhibit an elongated morphology with pronounced actinin striation and troponin-t expression.

Conclusions

In summary, a bioinspired, mechanically rigid and conductive Fmoc-FF-PAni hydrogel was fabricated by *in situ* polymerization of Ani inside the Fmoc-FF hydrogel matrix. The structural and morphological analyses indicate that the Fmoc-FF-PAni fibers are composed of both Fmoc-FF and PAni. Interestingly, unlike most previous studies, the conducting emeraldine salt form of PAni is obtained without the use of additional inorganic or organic acids. The Fmoc-FF-PAni hydrogels are mechanically rigid showing a G' value of ~2 MPa, much higher than previously reported for supramolecular or peptide-based hydrogels. Importantly, the Fmoc-FF-PAni hydrogels are capable of self-healing, as demonstrated by the quick fusion of two separated hydrogel blocks without any external healing agent. As a consequence of ample intrinsic doping, dried Fmoc-FF-PAni hydrogels exhibited ohmic nature in their I–V curves, with a DC conductance of 0.5 mS. Intriguingly, these hydrogels also showed self-healing conductivity in their hydrated form, i.e., retained their bulk conductivity after being cut into two blocks and rejoined. Combining both conductivity and elasticity, the Fmoc-FF-PAni hydrogels were employed to construct a pressure sensor device with a sensitivity of ~15–51 kPa^{-1} at pressure values < 330 Pa. Finally, their integrated biocompatibility, conductivity, and soft nature allowed for their application as a soft substrate for the growth of functioning electrogenic cardiac cells. Moreover, the self-healing property of the Fmoc-FF-PAni hydrogels may potentially allow them to endure the continuous contractions of the heart, making them intriguing candidates to serve as cardiac cell delivery vehicles. Importantly, the mechanical properties of these hydrogels could be tuned by altering the gelator (Fmoc-FF) concentration, as demonstrated here for two different applications. Accordingly, for pressure sensing, a higher peptide concentration was used (2% (w/v)), while for cell growth, a lower concentration was used (0.5% (w/v)). Thus,

the Fmoc-FF-PAni hydrogels provide a tunable, biocompatible, conducting, and self-healing platform for biomedical and various other applications.

Methods and Experimental Details

Hydrogel Preparation

Lyophilized Fmoc-FF (Bachem, Budendorf, Switzerland) was dissolved in DMSO at a concentration of 100 mg mL^{-1}. The Fmoc-FF hydrogels were prepared by diluting this stock solution in ultrapure water (Biological Industries, Beit Haemeck, Israel). To prepare the composite hydrogels, the required quantity of Ani (ACS reagent, Sigma-Aldrich) was first homogeneously solubilized in water by rigorous vortexing. The Fmoc-FF stock solution was then diluted in this aqueous solution of Ani to yield the Fmoc-FF-Ani gel. The final Fmoc-FF concentration in both gels was 0.5% (w/v), unless otherwise mentioned. The molar ratio of Fmoc-FF to Ani was maintained as 1:5 in all experiments, unless otherwise mentioned. Ani was then polymerized by an aqueous solution of APS (Sigma-Aldrich, molar ratio of APS:Ani = 3:1). For rheology, pressure sensing, and biological applications, hydrogel scaffolds were prepared. For this purpose, the gels were allowed to form in plastic syringes (internal diameter = 8 mm) and were taken out by cutting the syringes. To produce the Fmoc-FF-PAni gel scaffolds, pre-prepared Fmoc-FF-Ani scaffolds were immersed in an APS solution of the required concentration. Fmoc-FF-PAni hydrogel scaffolds were purified by immersing in ddH_2O with continuous shaking for 3 days. Water was changed twice a day. For biological applications, the Fmoc-FF-PAni hydrogel scaffolds were washed with ethanol and PBS for 2 h each, followed by purification in ddH_2O for 3 days.

Fourier Transform Infrared (FTIR) Spectroscopy

To obtain the FTIR spectra, 30 μL of the hydrogels were deposited onto disposable KBr infrared sample cards (Sigma-Aldrich, Rehovot, Israel), which were then allowed to dry under vacuum. The measurements were carried out in a nitrogen purged Nexus 470 FTIR spectrometer (Nicolet, Offenbach, Germany) equipped with a deuterated triglycine sulfate (DTGS) detector.

UV–Vis Spectra

UV–vis spectra of the samples were recorded in a T60 UV–vis spectrophotometer (PG instruments). A quartz cuvette with an optical path length of 1 mm was used. For the concentration dependent UV–vis measurements, the samples with variable Fmoc-FF concentrations were prepared according to the method described in the Hydrogel Preparation section. To obtain the UV–vis spectra of Fmoc-FF-PAni, a pre-prepared Fmoc-FF-PAni hydrogel with 0.5% Fmoc-FF concentration was dispersed in ddH_2O.

Fluorescence Spectra

Fluorescence spectra of the samples were recorded using a Horiba Jobin Yvon FL3-11 fluorimeter (Horiba Jobin Yvon, NJ, U.S.A.). The samples were prepared in quartz cells of 1 cm path length and excited at 280 nm. Emission scans were recorded using 5 nm excitation and emission slits. For the concentration dependent fluorescence measurements, the samples

with variable Fmoc-FF concentrations were prepared according to the method described in the Hydrogel Preparation section.

Transmission Electron Microscopy (TEM)

Hydrogel samples of 10 μL were drop-casted onto 400-mesh copper grids covered by a carbon-stabilized Formvar film (SPI, West Chester, PA, U.S.A.). The samples were dried under ambient conditions, and the micrographs were recorded using a JEM-1400Plus transmission electron microscope (JEM) operating at 80 kV. The diameter of the hydrogel nanofibers was calculated from the respective TEM images.

Rheological Analysis

A peptide concentration of 2% (w/v) was used if not otherwise mentioned, whereas the molar ratio of Fmoc-FF:Ani was maintained fixed (1:5). The rheological studies of the hydrogel scaffolds were performed on an ARES-G2 rheometer (TA Instruments, New Castle, DE, U.S.A.) using an 8 mm parallel-plate geometry with a gap of 1000 μm. We have repeated the measurements with at least three independent samples to ensure reproducibility.

Conductivity Analysis

The hydrogels were drop-casted on pre-fabricated field-effect transistor substrates (Ossila, U.K.) with a varying electrode gap of 5, 10, and 20 μm and dried under ambient conditions. Current–voltage (I–V) measurements were performed on a Keithley 4200-SCS source-meter using the two-probe method. All measurements were carried out from –1 to 1 V with 0.05 V steps, and 0.1 s hold time and sweep delay. Conductance values were extracted from the slope of the linear curves. We have repeated the measurements with at least three independent samples to ensure reproducibility.

Electrochemical Analysis

Cyclic voltammetry (CV) was performed using an electrochemical station (CHI600E; CH Instrument, Austin, TX, U.S.A.) in three electrode configuration in 0.5 M H_2SO_4 electrolyte at a sweep rate of 100 mV s^{-1}. The three-electrode system consists of Fmoc-FF-PAni hydrogel-loaded glassy carbon electrode (GCE) as the working electrode, saturated Ag/AgCl as the reference electrode, and Pt wire as the counter electrode.

Pressure-Dependent Resistance Measurements

The Fmoc-FF-PAni hydrogel scaffolds (diameter = 8 mm, height = 3 mm) were placed on an ~1 mm gap between copper electrodes adhered to a glass slide and connected to a digital multimeter (TES-2732; TES Electrical Electronic Corp., Taiwan). The scaffolds were compressed using an Instron 4502 machine with a load cell of 100 N at a compression rate of 1 mm min^{-1}, and the resistance values were simultaneously recorded. DC conductivity (σ) was calculated according to the relation

$$\sigma = (1/R)(d/a)$$

where R is the resistance, a is the area of the electrode, and d is the thickness of the sample. We have repeated the measurements with at least three independent samples to ensure reproducibility.

Cardiac Cell Isolation, Seeding, and Cultivation

Cardiac cells were isolated according to Tel Aviv University ethical use protocols, as previously described.76 Left ventricles of 0–3-day-old neonatal Sprague–Dawley rats were harvested, and cells were isolated by six cycles (30 min each) of enzyme digestion using collagenase type II (95 U/mL; Worthington, Lakewood, NJ, U.S.A.) and pancreatin (0.6 mg/mL; Sigma-Aldrich) in DMEM. After each round of digestion, the cells were centrifuged (600g, 5 min, 4 °C) and resuspended in M-199 culture medium (Biological Industries, Beit Haemeck, Israel) supplemented with 0.6 mM $CuSO_4{\cdot}5H_2O$, 0.5 mM $ZnSO_4{\cdot}7H_2O$, 1.5 mM vitamin B12, 500 U/mL Penicillin, 100 mg/mL streptomycin, and 0.5% (v/v) fetal bovine serum (FBS). To enrich the cardiomyocyte population, cells were suspended in culture medium with 5% FBS and pre-plated twice (50 min). Cell number and viability were determined by hemocytometer and trypan blue exclusion assay.

The 5×10^5 cardiac cells in a volume of 20 μL were seeded onto the hydrogels, followed by 40 min of incubation (humidity incubator, 37 °C, 5% CO_2). The cells were then supplemented with culture medium (5% FBS) and further cultivated.

Calcium Imaging

Seven days after seeding on the hydrogel surface, the cells were incubated with 10 μM fluo-4 AM (Invitrogen, Carlsbad, CA, U.S.A.) and 0.1% Pluronic F-127 (Sigma-Aldrich) for 45 min at 37 °C. The samples were then washed with medium and imaged using an inverted fluorescence microscope (Eclipse TI; Nikon, Tokyo, Japan). Videos were acquired using an ORCA-Flash 4.0 v2 digital complementary metal-oxide semiconductor (CMOS) camera (Hamamatsu photonics, Hamamatsu city, Japan) at 100 frames s^{-1}. Videos were analyzed using the ImageJ software (NIH, Bethesda, MD, U.S.A.).We have repeated the measurements with at least three independent samples to ensure reproducibility.

Immunostaining

Immunostaining was performed as previously described.77 Cardiac cell constructs were fixed and permeabilized in 100% cold methanol for 10 min, washed three times in PBS, and then blocked for 1 h at room temperature in PBS containing 2% FBS, after which the samples were washed three times. The samples were then incubated for 90 min with primary antibodies to detect α-sarcomeric actinin (1:750, Sigma-Aldrich) or troponin (1:200, Abcam), washed three times, and incubated for 1 h with Alexa Fluor 647 conjugated goat anti-mouse antibody (1:500; Jackson Immunoresearch Laboratories) and Alexa Fluor 488 conjugated goat anti-rabbit antibody (1:500; Jackson Immunoresearch Laboratories). For nuclei detection, the cells were incubated for 3 min with Hoechst 33258 (1:10; Sigma-Aldrich) and washed three times. Samples were visualized with a scanning laser confocal microscope (Eclipse Ni, Nikon). We have repeated the measurements with at least three independent samples to ensure reproducibility.

Supplementary Material

Refer to Web version on PubMed Central for supplementary material.

Acknowledgments

This work was partially supported by grants from the European Research Council under the European Union's Horizon 2020 research and innovation program (BISON, Advanced ERC grant, no. 694426) (E.G.). P.C. gratefully acknowledges the Center for Nanoscience and Nanotechnology of Tel Aviv University for financial support. The authors thank Sigal Rencus-Lazar for linguistic editing and the members of the Gazit laboratory for helpful discussions.

References

(1). Kopecek J. Swell Gels. Nature. 2002; 417:388–391. [PubMed: 12024197]

(2). Cushing MC, Anseth KS. Hydrogel Cell Cultures. Science. 2007; 316:1133–1134. [PubMed: 17525324]

(3). Williams RJ, Smith AM, Collins R, Hodson N, Das AK, Ulijn RV. Enzyme-assisted Self-assembly under Thermodynamic Control. Nat Nanotechnol. 2009; 4:19–24. [PubMed: 19119277]

(4). Seliktar D. Designing Cell-compatible Hydrogels for Biomedical Applications. Science. 2012; 336:1124–1128. [PubMed: 22654050]

(5). Du XW, Zhou J, Shi JF, Xu B. Supramolecular Hydrogelators and Hydrogels: from Soft Matter to Molecular Biomaterials. Chem Rev. 2015; 115:13165–13307. [PubMed: 26646318]

(6). Urakami H, Guan Z. Living Ring-Opening Polymerization of a Carbohydrate-Derived Lactone for the Synthesis of Protein-Resistant Biomaterials. Biomacromolecules. 2008; 9:592–597. [PubMed: 18220347]

(7). Fleming S, Ulijn RV. Design of Nanostructures Based on Aromatic Peptide Amphiphiles. Chem Soc Rev. 2014; 43:8150–8177. [PubMed: 25199102]

(8). Fichman G, Gazit E. Self-assembly of Short Peptides to Form Hydrogels: Design of Building Blocks, Physical Properties and Technological Applications. Acta Biomater. 2014; 10:1671–1682. [PubMed: 23958781]

(9). Adhikari B, Banerjee A. Short-Peptide-Based Hydrogel: A Template for the *In Situ* Synthesis of Fluorescent Silver Nanoclusters by Using Sunlight. Chem - Eur J. 2010; 16:13698–13705. [PubMed: 20945315]

(10). Adams DJ. Dipeptide and Tripeptide Conjugates as Low-Molecular-Weight Hydrogelators. Macromol Biosci. 2011; 11:160–173. [PubMed: 21080382]

(11). Adams DJ, Mullen LM, Berta M, Chen L, Frith WJ. Relationship between Molecular Structure, Gelation Behaviour and Gel Properties of Fmoc-Dipeptides. Soft Matter. 2010; 6:1971–1980.

(12). Mahler A, Reches M, Rechter M, Cohen S, Gazit E. Rigid, Self-Assembled Hydrogel Composed of a Modified Aromatic Dipeptide. Adv Mater. 2006; 18:1365–1370.

(13). Jayawarna V, Ali M, Jowitt TA, Miller AF, Saiani A, Gough JE, Ulijn RV. Nanostructured Hydrogels for Three-Dimensional Cell Culture through Self-Assembly of Fluorenylmethoxycarbonyl-Dipeptides. Adv Mater. 2006; 18:611–614.

(14). Dou X-Q, Feng C-L. Amino Acids and Peptide-Based Supramolecular Hydrogels for Three-Dimensional Cell Culture. Adv Mater. 2017; 29

(15). Zhou M, Smith AM, Das AK, Hodson NW, Collins RF, Ulijn RV, Gough JE. Self-Assembled Peptide-Based Hydrogels as Scaffolds for Anchorage-Dependent Cells. Biomaterials. 2009; 30:2523–2530. [PubMed: 19201459]

(16). Guimard NK, Gomez N, Schmidt CE. Conducting Polymers in Biomedical Engineering. Prog Polym Sci. 2007; 32:876–921.

(17). Baheiraei N, Yeganeh H, Ai J, Gharibi R, Azami M, Faghihi F. Synthesis, Characterization and Antioxidant Activity of a Novel Electroactive and Biodegradable Polyurethane for Cardiac Tissue Engineering Application. Mater Sci Eng, C. 2014; 44:24–37.

(18). Xia Y, Zhu H. Polyaniline Nanofiber-Reinforced Conducting Hydrogel with Unique pH-Sensitivity. Soft Matter. 2011; 7:9388–9393.

(19). Xiao Y, He L, Che J. An Effective Approach for the Fabrication of Reinforced Composite Hydrogel Engineered with Swnts, Polypyrrole and PEGDA Hydrogel. J Mater Chem. 2012; 22:8076–8082.

(20). Wu Y, Chen YX, Yan J, Yang S, Dong P, Soman P. Fabrication of Conductive Polyaniline Hydrogel Using Porogen Leaching and Projection Microstereolithography. J Mater Chem B. 2015; 3:5352–5360.

(21). Kishi R, Kubota K, Miura T, Yamaguchi T, Okuzaki H, Osada Y. Mechanically Tough Double-Network Hydrogels with High Electronic Conductivity. J Mater Chem C. 2014; 2:736–743.

(22). Kishi R, Hiroki K, Tominaga T, Sano K-I, Okuzaki H, Martinez JG, Otero TF, Osada Y. Electro-Conductive Double-Network Hydrogels. J Polym Sci, Part B: Polym Phys. 2012; 50:790–796.

(23). Pan L, Yu G, Zhai D, Lee HR, Zhao W, Liu N, Wang H, Tee BC-K, Shi Y, Cui Y, Bao Z. Hierarchical Nanostructured Conducting Polymer Hydrogel with High Electrochemical Activity. Proc Natl Acad Sci U S A. 2012; 109:9287–9292. [PubMed: 22645374]

(24). Schmidt CE, Shastri VR, Vacanti JP, Langer R. Stimulation of Neurite Outgrowth using an Electrically Conducting Polymer. Proc Natl Acad Sci U S A. 1997; 94:8948–8953. [PubMed: 9256415]

(25). Li L, Wang Y, Pan L, Shi Y, Cheng W, Shi Y, Yu G. A Nanostructured Conductive Hydrogels-Based Biosensor Platform for Human Metabolite Detection. Nano Lett. 2015; 15:1146–1151. [PubMed: 25569673]

(26). Zhai D, Liu B, Shi Y, Pan L, Wang Y, Li W, Zhang R, Yu G. Highly Sensitive Glucose Sensor Based on Pt Nanoparticle/Polyaniline Hydrogel Heterostructures. ACS Nano. 2013; 7:3540–3546. [PubMed: 23472636]

(27). Ding H, Zhong M, Kim YJ, Pholpabu P, Balasubramanian A, Hui CM, He H, Yang H, Matyjaszewski K, Bettinger CJ. Biologically Derived Soft Conducting Hydrogels using Heparin-Doped Polymer Networks. ACS Nano. 2014; 8:4348–4357. [PubMed: 24738911]

(28). Dong R, Zhao X, Guo B, Ma PX. Self-Healing Conductive Injectable Hydrogels with Antibacterial Activity as Cell Delivery Carrier for Cardiac Cell Therapy. ACS Appl Mater Interfaces. 2016; 8:17138–17150. [PubMed: 27311127]

(29). Dvir T, Timko BP, Brigham MD, Naik SR, Karajanagi SS, Levy O, Jin H, Parker KK, Langer R, Kohane DS. Nanowired Three-Dimensional Cardiac Patches. Nat Nanotechnol. 2011; 6:720–725. [PubMed: 21946708]

(30). Yan X, Chen J, Yang J, Xue Q, Miele P. Fabrication of Free-Standing, Electrochemically Active, and Biocompatible Graphene Oxide-Polyaniline and Graphene-Polyaniline Hybrid Papers. ACS Appl Mater Interfaces. 2010; 2:2521–2529. [PubMed: 20735069]

(31). Hsiao C-W, Bai M-Y, Chang Y, Chung M-F, Lee T-Y, Wu C-T, Maiti B, Liao Z-X, Li R-K, Sung HW. Electrical Coupling of Isolated Cardiomyocyte Clusters Grown on Aligned Conductive Nanofibrous Meshes for Their Synchronized Beating. Biomaterials. 2013; 34:1063–1072. [PubMed: 23164424]

(32). Chakraborty P, Bairi P, Roy B, Nandi AK. Improved Mechanical and Electronic Properties of Co-Assembled Folic Acid Gel with Aniline and Polyaniline. ACS Appl Mater Interfaces. 2014; 6:3615–3622. [PubMed: 24495072]

(33). Ryu J, Park CB. Synthesis of Diphenylalanine/Polyaniline Core/Shell Conducting Nanowires by Peptide Self-Assembly. Angew Chem, Int Ed. 2009; 48:4820–4823.

(34). Li D, Huang J, Kaner RB. Polyaniline Nanofibers: A Unique Polymer Nanostructure for Versatile Applications. Acc Chem Res. 2009; 42:135–145. [PubMed: 18986177]

(35). Wei D, Lin X, Li L, Shang S, Yuen MC-w, Yan G, Yu X. Controlled Growth of Polypyrrole Hydrogels. Soft Matter. 2013; 9:2832–2836.

(36). Conte MP, Singh N, Sasselli IR, Escuder B, Ulijn RV. Metastable Hydrogels from Aromatic Dipeptides. Chem Commun. 2016; 52:13889–13892.

(37). Rana U, Chakrabarti K, Malik S. Benzene Tetracarboxylic Acid Doped Polyaniline Nanostructures: Morphological, Spectroscopic and Electrical Characterization. J Mater Chem. 2012; 22:15665–15671.

(38). Garai A, Kuila BK, Nandi AK. Montmorillonite Clay Nanocomposites of Sulfonic Acid Doped Thermoreversible Polyaniline Gel: Physical and Mechanical Properties. Macromolecules. 2006; 39:5410–5418.

(39). Deore BA, Yu I, Freund MS. A Switchable Self-Doped Polyaniline: Interconversion between Self-Doped and Non-Self-Doped Forms. J Am Chem Soc. 2004; 126:52–53. [PubMed: 14709055]

(40). Tang C, Ulijn RV, Saiani A. Effect of Glycine Substitution on Fmoc-Diphenylalanine Self-Assembly and Gelation Properties. Langmuir. 2011; 27:14438–14449. [PubMed: 21995651]

(41). Yan X, Cui Y, He Q, Wang K, Li J. Organogels based on Self-Assembly of Diphenylalanine Peptide and their Application to Immobilize Quantum Dots. Chem Mater. 2008; 20:1522–1526.

(42). Colquhoun C, Draper ER, Schweins R, Marcello M, Vadukul D, Serpell LC, Adams DJ. Controlling the Network Type in Self-Assembled Dipeptide Hydrogels. Soft Matter. 2017; 13:1914–1919. [PubMed: 28186211]

(43). Sangeetha NM, Maitra U. Supramolecular Gels: Functions and Uses. Chem Soc Rev. 2005; 34:821–836. [PubMed: 16172672]

(44). Banerjee S, Das RK, Maitra U. Supramolecular Gels 'in Action'. J Mater Chem. 2009; 19:6649–6687.

(45). Kleinsmann AJ, Nachtsheim BJ. Phenylalanine-Containing Cyclic Dipeptides – The Lowest Molecular Weight Hydrogelators based on Unmodified Proteinogenic Amino Acids. Chem Commun. 2013; 49:7818–7820.

(46). Khalily MA, Goktas M, Guler MO. Tuning Viscoelastic Properties of Supramolecular Peptide Gels *via* Dynamic Covalent Crosslinking. Org Biomol Chem. 2015; 13:1983–1987. [PubMed: 25566850]

(47). Pashuck ET, Cui HG, Stupp SI. Tuning Supramolecular Rigidity of Peptide Fibers through Molecular Structure. J Am Chem Soc. 2010; 132:6041–6046. [PubMed: 20377229]

(48). Martin AD, Robinson AB, Mason AF, Wojciechowski JP, Thordarson P. Exceptionally Strong Hydrogels through Self-Assembly of an Indole-Capped Dipeptide. Chem Commun. 2014; 50:15541–15544.

(49). Halperin-Sternfeld M, Ghosh M, Sevostianov R, Grigoriants I, Adler-Abramovich L. Molecular Co-Assembly as a Strategy for Synergistic Improvement of the Mechanical Properties of Hydrogels. Chem Commun. 2017; 53:9586–9589.

(50). Calvert P. Hydrogels for Soft Machines. Adv Mater. 2009; 21:743–756.

(51). Mukhopadhyay P, Fujita N, Takada A, Kishida T, Shirakawa M, Shinkai S. Regulation of A Real-Time Self-Healing Process in Organogel Tissues by Molecular Adhesives. Angew Chem, Int Ed. 2010; 49:6338–6342.

(52). Wang L, Wu Y, Hu T, Guo B, Ma PX. Electrospun Conductive Nanofibrous Scaffolds for Engineering Cardiac Tissue and 3D Bioactuators. Acta Biomater. 2017; 59:68–81. [PubMed: 28663141]

(53). Nyström G, Fernández-Ronco MP, Bolisetty S, Mazzotti M, Mezzenga R. Amyloid Templated Gold Aerogels. Adv Mater. 2016; 28:472–478. [PubMed: 26592185]

(54). Pan L, Chortos A, Yu G, Wang Y, Isaacson S, Allen R, Shi Y, Dauskardt R, Bao Z. An Ultra-Sensitive Resistive Pressure Sensor Based on Hollow-Sphere Microstructure Induced Elasticity in Conducting Polymer Film. Nat Commun. 2014; 5:3002. [PubMed: 24389734]

(55). Si Y, Wang L, Wang X, Tang N, Yu J, Ding B. Ultrahigh-Water-Content, Superelastic, and Shape-Memory Nanofiber-Assembled Hydrogels Exhibiting Pressure-Responsive Conductivity. Adv Mater. 2017; 29

(56). Kharaziha M, Nikkhah M, Shin SR, Annabi N, Masoumi N, Gaharwar AK, Camci-Unal G, Khademhosseini A. Pgs: Gelatin Nanofibrous Scaffolds with Tunable Mechanical and Structural Properties for Engineering Cardiac Tissues. Biomaterials. 2013; 34:6355–6366. [PubMed: 23747008]

(57). Orlova Y, Magome N, Liu L, Chen Y, Agladze K. Electrospun Nanofibers as a Tool for Architecture Control in Engineered Cardiac Tissue. Biomaterials. 2011; 32:5615–5624. [PubMed: 21600646]

(58). Zong X, Bien H, Chung C-Y, Yin L, Fang D, Hsiao BS, Chu B, Entcheva E. Electrospun Fine-Textured Scaffolds for Heart Tissue Constructs. Biomaterials. 2005; 26:5330–5338. [PubMed: 15814131]

(59). Haraguchi Y, Shimizu T, Yamato M, Kikuchi A, Okano T. Electrical Coupling of Cardiomyocyte Sheets Occurs Rapidly *via* Functional Gap Junction Formation. Biomaterials. 2006; 27:4765–4774. [PubMed: 16737736]

(60). Noorman M, van der Heyden MA, van Veen TA, Cox MG, Hauer RN, de Bakker JM, van Rijen HV. Cardiac Cell-Cell Junctions in Health and Disease: Electrical *versus* Mechanical Coupling. J Mol Cell Cardiol. 2009; 47:23–31. [PubMed: 19344726]

(61). Dvir T, Benishti N, Shachar M, Cohen S. A Novel Perfusion Bioreactor Providing a Homogenous Milieu for Tissue Regeneration. Tissue Eng. 2006; 12:2843–2852. [PubMed: 17518653]

(62). Dvir T, Tsur-Gang O, Cohen S. Designer" Scaffolds for Tissue Engineering and Regeneration. Isr J Chem. 2005; 45:487–494.

(63). Bursac N, Loo YH, Leong K, Tung L. Novel Anisotropic Engineered Cardiac Tissues: Studies of Electrical Propagation. Biochem Biophys Res Commun. 2007; 361:847–853. [PubMed: 17689494]

(64). You JO, Rafat M, Ye GJ, Auguste DT. Nanoengineering the Heart: Conductive Scaffolds Enhance Connexin 43 Expression. Nano Lett. 2011; 11:3643–3648. [PubMed: 21800912]

(65). Shin SR, Jung SM, Zalabany M, Kim K, Zorlutuna P, Kim SB, Nikkhah M, Khabiry M, Azize M, Kong J, Wan KT, et al. Carbon-Nanotube-Embedded Hydrogel Sheets for Engineering Cardiac Constructs and Bioactuators. ACS Nano. 2013; 7:2369–2380. [PubMed: 23363247]

(66). Martinelli V, Cellot G, Toma FM, Long CS, Caldwell JH, Zentilin L, Giacca M, Turco A, Prato M, Ballerini L, Mestroni L. Carbon Nanotubes Instruct Physiological Growth and Functionally Mature Syncytia: Nongenetic Engineering of Cardiac Myocytes. ACS Nano. 2013; 7:5746–5756. [PubMed: 23734857]

(67). Annabi N, Shin SR, Tamayol A, Miscuglio M, Bakooshli MA, Assmann A, Mostafalu P, Sun JY, Mithieux S, Cheung L, Tang XS, et al. Highly Elastic and Conductive Human-Based Protein Hybrid Hydrogels. Adv Mater. 2016; 28:40–49. [PubMed: 26551969]

(68). Discher DE, Janmey P, Wang Y-l. Tissue Cells Feel and Respond to the Stiffness of their Substrate. Science. 2005; 310:1139–1143. [PubMed: 16293750]

(69). Fleischer S, Shapira A, Feiner R, Dvir T. Modular Assembly of Thick Multifunctional Cardiac Patches. Proc Natl Acad Sci U S A. 2017; 114:1898–1903. [PubMed: 28167795]

(70). Versaevel M, Grevesse T, Gabriele S. Spatial Coordination between Cell and Nuclear Shape within Micropatterned Endothelial Cells. Nat Commun. 2012; 3:671. [PubMed: 22334074]

(71). Bray M-AP, Adams WJ, Geisse NA, Feinberg AW, Sheehy SP, Parker KK. Nuclear Morphology and Deformation in Engineered Cardiac Myocytes and Tissues. Biomaterials. 2010; 31:5143–5150. [PubMed: 20382423]

(72). Li M, Guo Y, Wei Y, MacDiarmid AG, Lelkes PI. Electrospinning Polyaniline-Contained Gelatin Nanofibers for Tissue Engineering Applications. Biomaterials. 2006; 27:2705–2715. [PubMed: 16352335]

(73). Nam H, An T, Lim G. Cell Behaviour on a Polyaniline Nanoprotrusion Structure Surface. Nanoscale Res Lett. 2014; 9:566. [PubMed: 25386102]

(74). Li W, Wan M. Porous Polyaniline Films with High Conductivity. Synth Met. 1998; 92:121–126.

(75). Das S, Chakraborty P, Ghosh R, Paul S, Mondal S, Panja A, Nandi AK. Folic Acid-Polyaniline Hybrid Hydrogel for Adsorption/Reduction of Chromium(VI) and Selective Adsorption of Anionic Dye from Water. ACS Sustainable Chem Eng. 2017; 5:9325–9337.

(76). Shevach M, Maoz BM, Feiner R, Shapira A, Dvir T. Nanoengineering Gold Particle Composite Fibers for Cardiac Tissue Engineering. J Mater Chem B. 2013; 1:5210–5217.

(77). Dvir T, Levy O, Shachar M, Granot Y, Cohen S. Activation of the ERK1/2 Cascade *via* Pulsatile Interstitial Fluid Flow Promotes Cardiac Tissue Assembly. Tissue Eng. 2007; 13:2185–2193. [PubMed: 17518740]

Europe PMC Funders Author Manuscripts

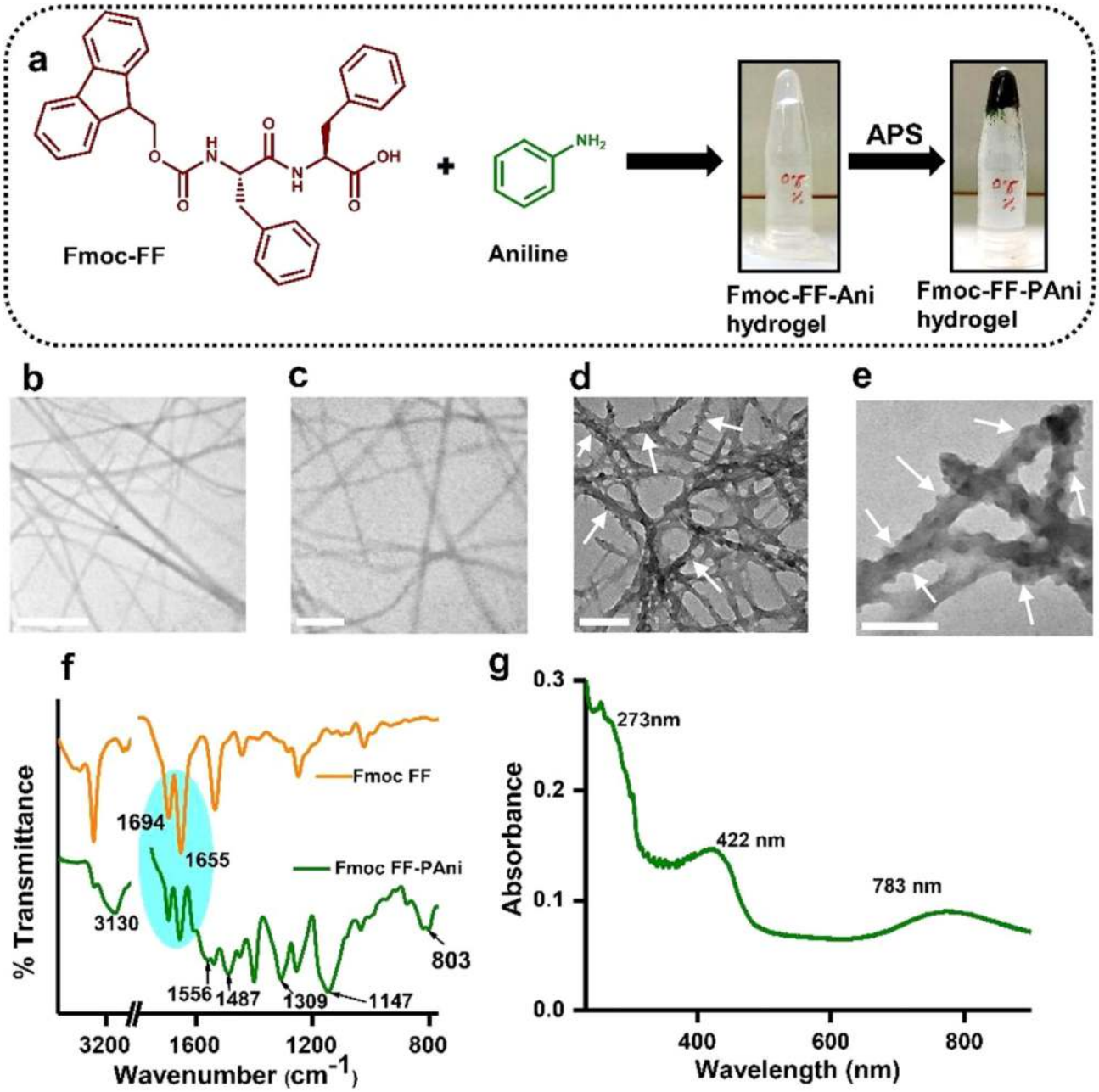

Figure 1.

Preparation and characterization of the Fmoc-FF-PAni hydrogels (Fmoc-FF concentration = 0.5% (w/v)). (a) Schematic representation of the formation of Fmoc-FF-PAni hydrogels by oxidative polymerization with APS. (b, c) TEM micrographs of the Fmoc-FF-Ani hydrogels. Scale bars are 500 and 200 nm for (b) and (c), respectively. (d, e) TEM micrographs of the Fmoc-FF-PAni hydrogels, showing fibers with a coarse surface. White arrows are drawn to guide the eye. Scale bars are 200 and 100 nm for (d) and (e), respectively. (f) FTIR spectra

of dried Fmoc-FF and Fmoc-FF-PAni hydrogels. (g) UV–vis spectra of a pulverized suspension of Fmoc-FF-PAni hydrogel in ddH_2O.

Europe PMC Funders Author Manuscripts

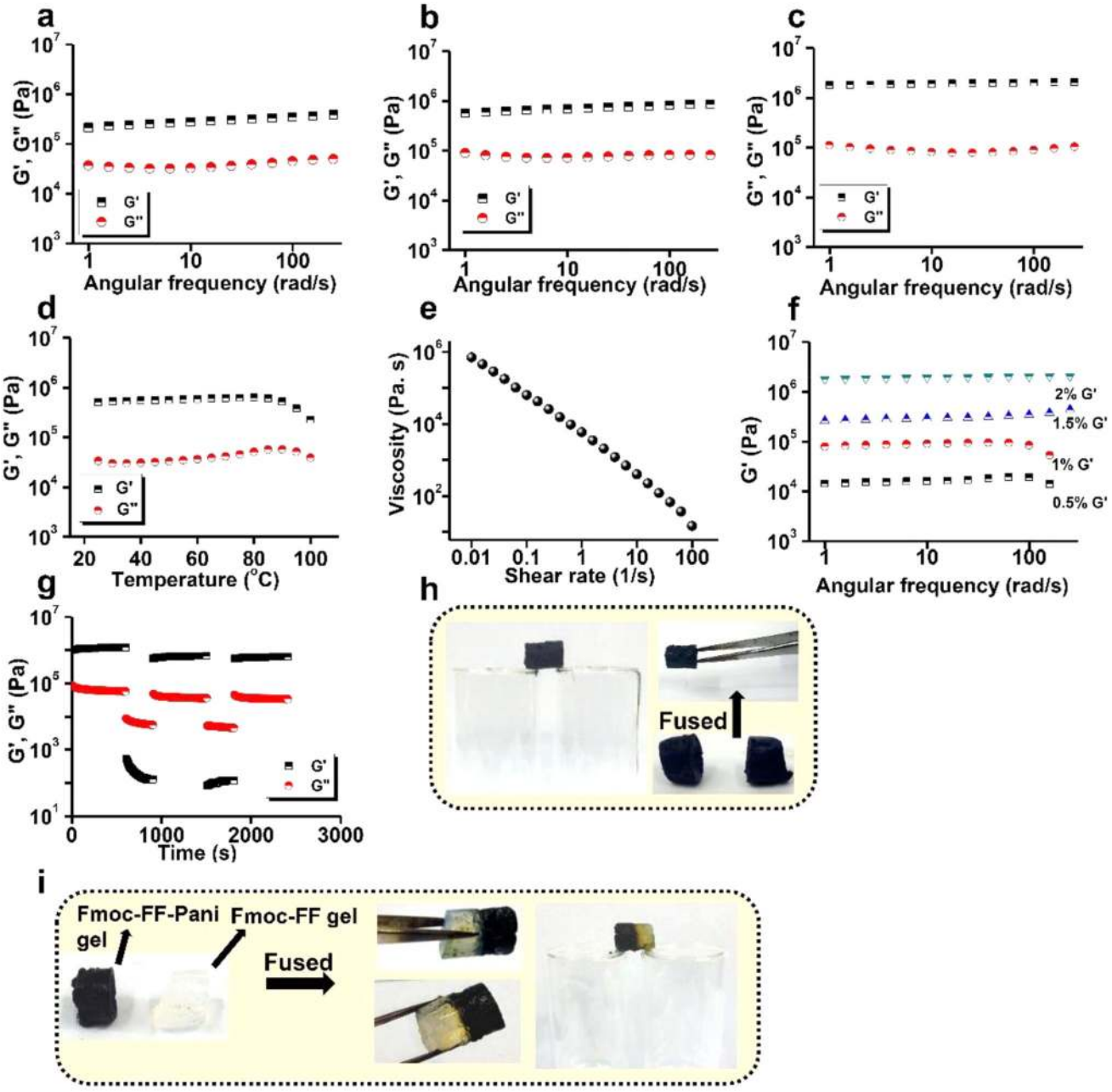

Figure 2.

Mechanical properties of the hydrogels at 25 °C. (a–c) Frequency-dependent oscillatory rheology of (a) Fmoc-FF, (b) Fmoc-FF-Ani, and (c) Fmoc-FF-PAni hydrogels (Fmoc-FF concentration = 2% (w/v)). (d) Storage and loss moduli of the Fmoc-FF-PAni hydrogels as a function of temperature (Fmoc-FF concentration = 2% (w/v)). (e) Shear viscosity vs shear rate plot of the Fmoc-FF-PAni hydrogels (Fmoc-FF concentration = 2% (w/v)). (f) Variation of G' with angular frequency forFmoc-FF-PAni hydrogels at different Fmoc-FF concentrations (w/v). (g) Continuous step strain measurement at alternate 0.1% and 100% strains over time for Fmoc-FF-PAni hydrogels (Fmoc-FF concentration = 2% (w/v)). (h, i)

Europe PMC Funders Author Manuscripts

Demonstration of the self-healing property (Fmoc-FF concentration = 2% (w/v)). (h) Two separated blocks of Fmoc-FF-PAni hydrogel healed after being kept in contact for 5 min. (i) Two separate blocks of Fmoc-FF and Fmoc-FF-PAni hydrogels healed after being kept in contact for 5 min.

Europe PMC Funders Author Manuscripts

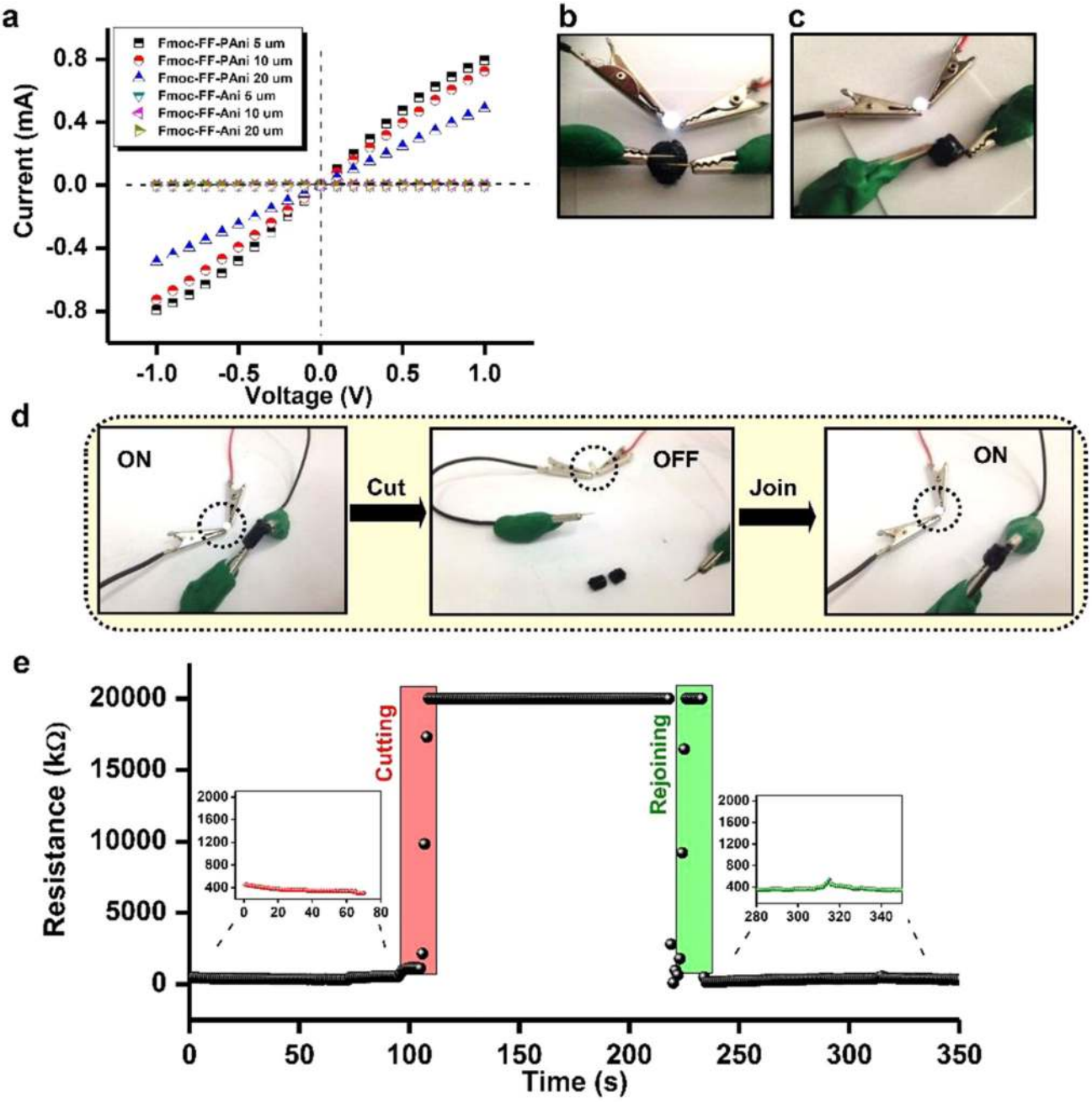

Figure 3.

Conducting properties of the Fmoc-FF-PAni hydrogels. (a) *I*–*V* characteristic curves of the dried Fmoc-FF-PAni and Fmoc-FF-Ani hydrogels measured between two gold pads separated by different gaps (5, 10, and 20 μm) (Fmoc-FF concentration = 0.5% (w/v)). (b, c) Depiction of conductivity of the Fmoc-FF-PAni hydrogels deployed as a bridge to complete an electrical circuit with a serially connected LED (Fmoc-FF concentration = 2% (w/v)). (d) Photographs showing the recurrence of bulk conductivity of the Fmoc-FF-PAni hydrogels after cutting and joining the monoliths with the "On" and "Off" state of the LED (Fmoc-FF

Europe PMC Funders Author Manuscripts

concentration = 2% (w/v)). (e) Real-time measurement of the resistance values of Fmoc-FF-PAni hydrogels during the cutting and rejoining procedure (Fmoc-FF concentration = 2% (w/v)).

Europe PMC Funders Author Manuscripts

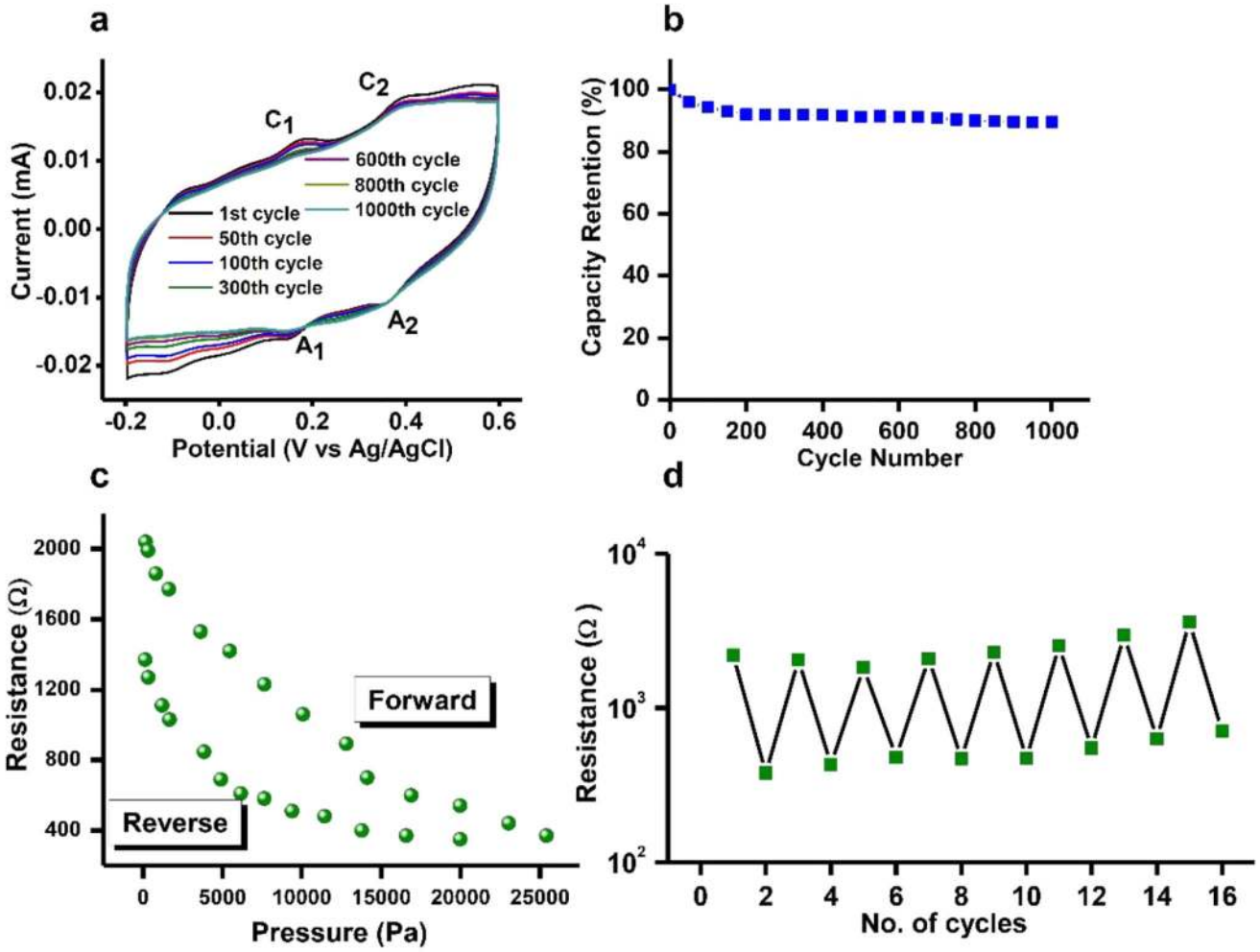

Figure 4.

(a, b) Electrochemical analysis of Fmoc-FF-PAni hydrogels (Fmoc-FF concentration = 0.5% (w/v)). (a) Cyclic voltammetry sweeps in 0.5 M H_2SO_4 at a scan rate of 100 mV s^{-1} and (b) capacity retention of ~89% at 1000th cycle. The data indicate stable and nearly repeatable redox properties of PAni in the Fmoc-FF-PAni hydrogel network system. (c, d) Application of the Fmoc-FF-PAni hydrogel as a pressure sensor device (Fmoc-FF concentration = 2% (w/v)). (c) Variation of the resistance of the Fmoc-FF-PAni hydrogel with applied pressure. (d) Repeated cycles of pressure responsive resistance manifested by the Fmoc-FF-PAni hydrogel-based sensor device.

Europe PMC Funders Author Manuscripts

Europe PMC Funders Author Manuscripts

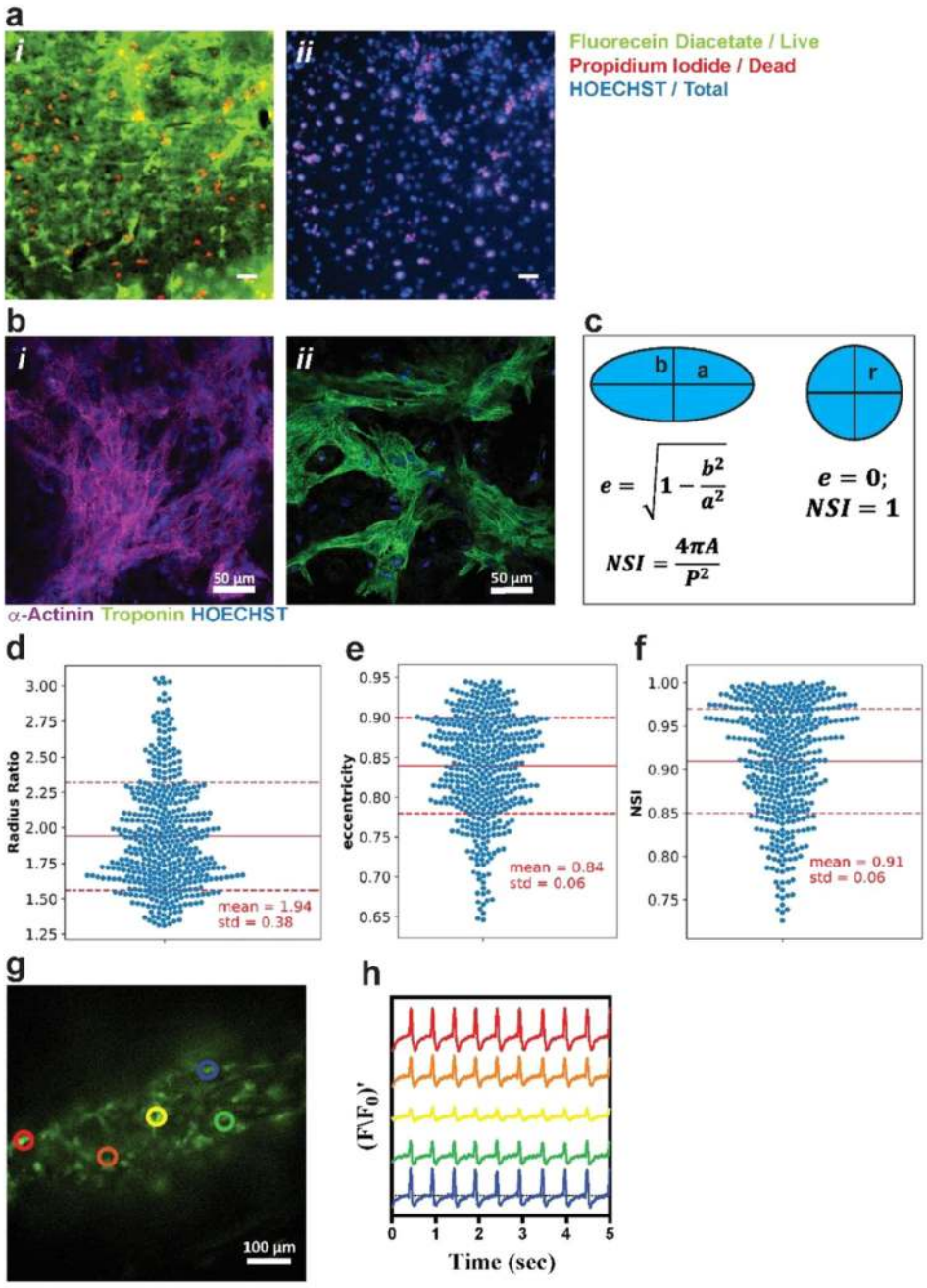

Figure 5.

Cardiac cell culture and function. (a) Cardiomyocyte viability by Live/Dead assay. (i) Live cells stained with fluorecein diacetate (green) and dead cell nuclei stained with PI (red). (ii) Hoechst (blue) and PI staining were used for quantifying viability. % Viability was quantified as the ratio of PI-negative nuclei to total nuclei count. % viability was 0.69 ± 0.013 as measured from two different samples, with 4 FOVs each. Scale bar, 50 μm. (b) Cardiac cell staining for alpha actinin (i, purple) and troponin-t (ii, green); nuclei are Hoechst-stained (blue). (c) Nuclear stains were used to quantify nuclear morphology.

Eccentricity, *e*, and nuclear shape index, NSI, were defined in order to assess whether nuclei were round or elliptical. Radius aspect ratio (d), eccentricity (e), and NSI (f) were calculated for nuclei from 8 images from two different samples. (g) Calcium transient was assessed at specified points by monitoring calcium dye fluorescence. (h) Synchronized calcium signals were observed at all points. F/F_0 refers to measured fluorescence normalized to maximum fluorescence. The colors are correlated to the colored circles in (g).

Europe PMC Funders Author Manuscripts

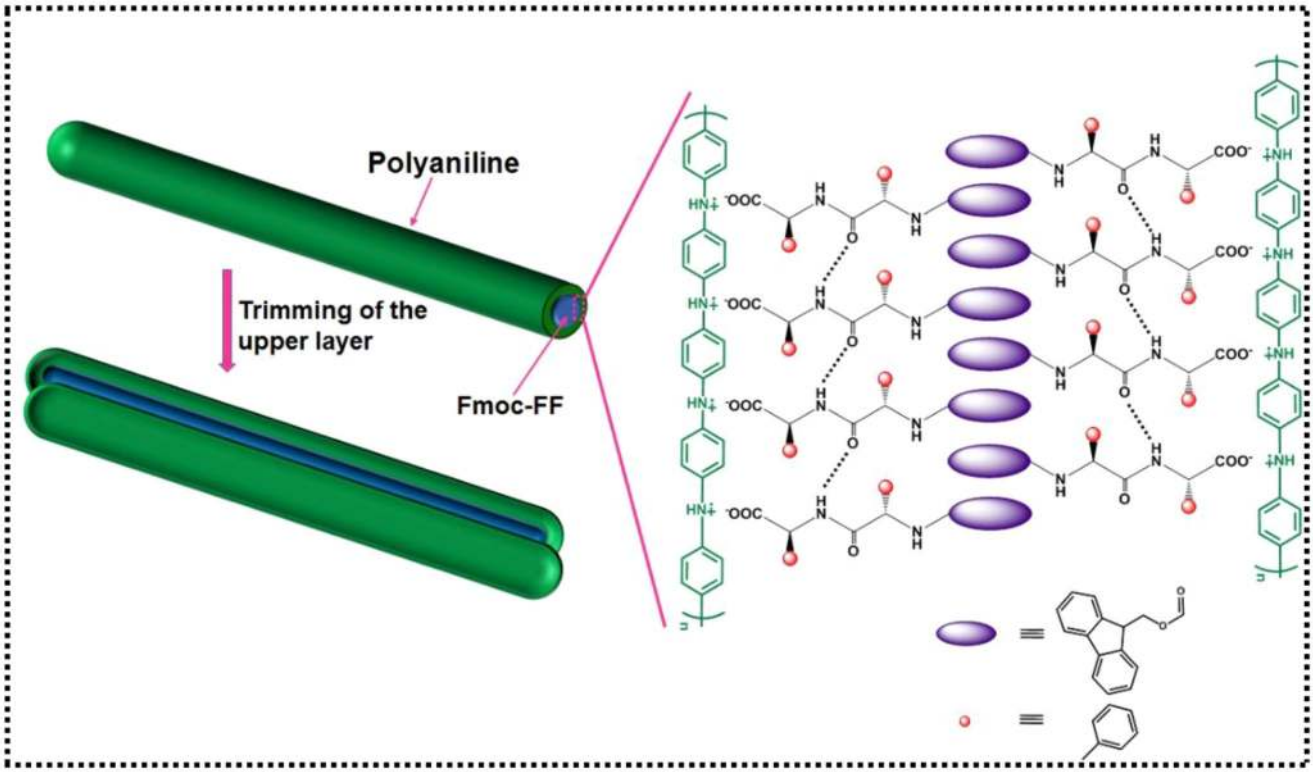

Scheme 1. Schematic Model of the Formation of the Fmoc-FF-PAni Fibers

Europe PMC Funders Author Manuscripts